Direct Evidence of Charge Transfer upon Anion Intercalation in Graphite Cathodes through New Electronic States: An Experimental and Theoretical study of Hexafluorophosphate

Tristan de Boer,[†,*] Jacob Lapping,[‡] Jeffrey A. Read,[§] Timothy T. Fister, [^] Mahalingam Balasubramanian,[¶] Jordi Cabana,[‡,*] Alexander Moewes[†]

†Department of Physics and Engineering Physics, University of Saskatchewan, 116 Science Place, Saskatoon, Saskatchewan, S7N 5E2, Canada

‡ Department of Chemistry, University of Illinois at Chicago, 845 W Taylor Street, Chicago, Illinois, 60607, USA

§ Sensors and Electron Devices Directorate, US Army Research Laboratory, 2800 Powder Mill Road, Adelphi, Maryland, 20783, USA

^ Chemical Sciences and Engineering Division, Argonne National Laboratory, 9700 S. Cass Avenue, Lemont, Illinois, 60439, USA

¶ Advanced Photon Source, Argonne National Laboratory, 9700 S. Cass Avenue, Lemont, Illinois, 60439, USA

ABSTRACT: Graphite intercalation compounds continue to be central to technologies for electrochemical energy storage, from anodes in established Li-ion batteries to cathodes in beyond Li-ion concepts paired with multivalent anodes. When used as a cathode, graphite intercalates a variety of anions, with PF_6^- being among the most common. Paired with Li intercalation at the anode, the corresponding dual carbon battery yields high energy and power densities. Given the available choice of anions as intercalants, it is important to elucidate how the graphite structure accommodates them in order to tailor the molecular species to maximize charge and reversibility. Yet the changes in electronic structure of the host graphite lattice upon anion intercalation are poorly understood compared to cations, which represent a fundamentally different reaction. In this work PF_6-intercalated graphite has been studied using techniques sensitive to electronic structure, namely x-ray Raman spectroscopy (XRS), x-ray absorption near-edge spectroscopy (XANES), and x-ray emission spectroscopy (XES). Complementary full-potential, all-electron density functional theory calculations yielded excellent agreement with the spectra, thus providing insight into charge compensation in the graphite lattice. In particular, a pre-π^* feature emerged in XRS/XANES which is direct evidence of removal of charge from the host lattice to compensate the intercalated anions, leading to an overall lowering of the Fermi energy level. This is expected to be characteristic of many intercalants in anion-intercalated graphite. The unambiguous identification of the origin of the pre- π^* spectral feature, which is frequently seen in graphitic systems, is of broad interest to the spectroscopy of graphitic systems, beyond the practical implications of anion-induced changes in the electronic properties for real devices.

INTRODUCTION

The electronic properties of graphite[1] can be tuned by perturbing the host lattice, including via functionalization,[2] substitutional doping,[3,4] intercalation,[5,6] and changing the dimensions to the nanoscopic regime.[7] Since 1841, graphite intercalated compounds (GICs) have been extensively studied leading to their use in thermal and electrical conductors, catalysis, and energy storage.[6] In particular, the Li GIC is extensively used today as the anode in Li-ion batteries,[8] which have pervasive applications in modern mobile electronics, and are increasingly employed for electric transportation, and grid storage. In the quest for low cost while preserving high energy density and minimizing environmental impact, graphite also emerges as the alternative intercalation host to the current transition-metal based cathodes. In such a dual-carbon battery, anions are intercalated into the graphite cathode during charging, generating a positive charge that can compensate the intercalation of Li^+ into the anode.[9] Anions that have been demonstrated for this purpose include ClO_4^-, BF_4^-, PF_6^-, $AlCl_4^-$, $CF_3SO_3^-$, and $(CF_3SO_2)_2N^-$, amongst others.[9–12] This reactivity is not unique to Li batteries, as $AlCl_4$-intercalated graphite has attracted considerable interest in next-generation non-aqueous Al batteries, where it is paired with the deposition of the trivalent metal on the anode.[13,14] Among all possible anion choices, PF_6^- has been studied extensively[15–24] because it produces a dual carbon battery with high storage capacity and favorable rate performance[10] with measured chemical diffusivity that compared well with lithium in cathodes such as $LiFePO_4$ or $LiCoO_2$. However, in comparison with the Li GIC, the fundamental processes underpinning reactivity remain poorly understood, particularly as it refers to the changes in crystal and electronic structure that graphite undergoes to accommodate the large molecular anion. The perturbation of the electronic structure, and the bonding interactions between host and guest species, determine the ability of charge carriers to conduct within the electrode structure, which, in turn, macroscopically determines energy utilization at high power density.

X-ray spectroscopy provides an established family of tools to probe the electronic structure of chemical compounds. Both x-ray absorption near-edge spectroscopy (XANES) and x-ray Raman spectroscopy (XRS) evaluate transitions from core to unoccupied states above the Fermi level characteristic of an element of interest, whereas occupied electronic states can be detected with x-ray emission spectroscopy (XES).[25] However, as it has been demonstrated for functionalized graphene oxide, the assignment of spectral features from XANES in extended systems cannot be simply decomposed by considering the coincidence of peaks from spectra in related compounds; rather, the electronic structure of the overall graphitic system must be considered.[2] Therefore, coupling measurements with computational modeling of the specific systems provides the highest and most detailed level of insight.

Here, we study PF_6-intercalated graphite electrodes using the full suite of XRS, XANES and XES. These spectra are subsequently interpreted by employing theoretical spectra calculated with density functional theory (DFT), using structural inputs from x-ray diffraction. Taken together, these techniques allow the structural and electronic properties of this material to be evaluated and discussed in the context of the expected functionality of the electrode. The spectra show that new unoccupied states are introduced above the Fermi level, in the form of a pre-π^* feature. While similar spectral weight before the π^* states has been observed in several instances, including irradiated graphite,[26] nanographite,[7] $FeCl_3$ intercalated graphite,[27] nanotubes,[28] and boron-doped graphite,[4] its origin remains elusive. For the irradiated and nanocarbon cases, it was attributed to sp^2 bond breaking and graphite edge states, emphasizing that the assignment of spectral features in the pre-π^* region cannot simply be done by considering their energetic position as spectral features at common energies may have differing origins. Our work unambiguously clarifies the underpinnings of this pre-π^* feature on the electronic structure upon intercalation, and suggests this is common to many anion-intercalated systems adding broad interest beyond the implications that affect the use of this material in real battery devices.

EXPERIMENTAL SECTION

Two forms of graphite electrodes were studied for this work. First, highly ordered pyrolytic graphite (HOPG) crystals (10 mm x 10 mm x 2 mm) from SPI Supplies were cleaved using a razor blade to approximately 0.2 mm thick. Subsequently, the crystals were made thinner by repeatedly peeling off single layers of graphite using adhesive tape until the total desired sample thickness was approximately 125 μm. Crystals of desired thickness were then individually weighed to determine galvanostatic cycling rate, and all crystals weighed between 10-15mg. HOPG crystals were used for XANES and XRS experiments. Additionally, mesocarbon microbeads (MCMB) type G-15 graphite powder was used to make electrode laminates. The electrode composite was generated using an N-methylpyrrolidine (NMP) based slurry. MCMB powder was combined with a polyvinylidene fluoride (PVDF) in NMP solution (6 wt.%) and carbon black in an 8:1:1 wt.% and cast onto an Al foil with a thickness of 6.0 mil using an adjustable film applicator. Laminates were dried for 30 min under a heat lamp, and then dried overnight in a vacuum oven at 100 °C. The dried laminates were subsequently punched to 0.5-inch diameter for use in electrochemical cells.

For electrochemical cycling, punched MCMB electrodes and cleaved HOPG electrodes were placed in the center of stainless steel CR2032 electrochemical cells, assembled, and sealed in an Ar-filled glovebox. Cells containing HOPG had a Pt contact welded to the bottom can to prevent stainless steel oxidation during electrochemical charging. Lithium metal was used as the counter and pseudo-reference electrode. The electrolyte solution was 2 M $LiPF_6$ in a 1:1 wt/wt mixture of fluoroethylene carbonate and ethylmethyl carbonate. A Celgard 2400 separator was placed between the working and counter-electrodes. Electrochemical cycling was performed galvanostatically at a rate of 0.05C, assuming a full charge capacity of 85 mAh/g, which corresponds to the intercalation of 0.23 PF_6^- ions per C_6 unit. Cells were halted at 5.2 V vs. Li^+/Li^0 at the end of the first charge cycle. After cycling, the cells were opened in a glovebox under argon and washed in anhydrous DMC to remove excess electrolyte. The electrodes were shipped to the beamline for measurement in an Ar-filled case rated for vacuum applications to minimize any contact with air or moisture.

X-ray diffraction measurements were performed on pristine and cycled MCMB electrodes to confirm the formation of the expected structure and evaluate phase purity. Patterns were collected between 10°-80°, 2θ, utilizing a step size of 0.02°, at a rate of 0.1°/min 2θ, in a custom air-free sample holder, using a Bruker D8 Advance diffractometer using Cu K radiation (λ = 1.5418 Å). Patterns were refined using the Pawley refinement method using GSAS-II. [29,30]

X-ray absorption near-edge spectroscopy (XANES) and x-ray emission spectroscopy (XES) are performed by promoting core electrons to the conduction band and monitoring their subsequent decay. Following excitation, electrons with sufficient energy may be ejected from the material, which can be monitored by measuring the ground current to the sample, yielding a total electron yield (TEY) measurement. XES measurements are performed by monitoring the core-hole decay using an energy-dispersive x-ray fluorescence spectrometer. In all cases, samples were loaded into the UHV sample chamber using an Ar-filled glove bag to avoid contamination due to their sensitivity to the laboratory atmosphere. XANES was performed at the C K-Edge at beamline 8-2 at the Stanford Synchrotron Light Source (SSRL, Menlo Park, CA). Two scans were performed on each sample, and scans were averaged to increase the signal to noise ratio. Energy references were collected using Fe simultaneously with the XANES for accurate energy alignment. C K-edge XES measurements were performed at beamline 8.0.1.1 of the Advanced Light Source (ALS, Lawrence Berkeley National Laboratory, CA). Non-resonant emission spectra were collected by exciting the sample at energies well above the excitation threshold. All measurements were performed with the sample mounted 45 ° to the incident beam. XES spectra were collected with the x-ray fluorescence spectrometer in a Rowland circle geometry oriented at a 90° angle to the incident radiation. The incident photon energy was calibrated using HOPG with an C K TEY XANES π^* peak value of 285.4 eV,[2] while the spectrometer energy was calibrated using elastic scattering features. The resolving power of the spectrometer ($E/\Delta E$) is 800.

X-ray Raman spectroscopy (XRS) was performed at Beamline 20-ID-B at the Advanced Photon Source. XRS is a technique that utilizes hard x-rays with a photon energy around 10 keV that penetrate approximately 2 mm into the sample. During the interaction with the sample, a fraction of the incident photons are inelastically scattered by exciting core electrons to the

valence band. The incident photon energy is varied and the intensity of inelastically scattered photons at a fixed energy is measured, so that the loss spectrum provides information similar to XANES to be collected. Since the origin of the signal is from inelastic scattering of hard x-rays, this technique is sensitive to the bulk properties of the material under observation. For each measurement, four HOPG electrodes, each cleaved to a sample thickness of 125 microns, were stacked in a glovebox with the H_2O and O_2 concentrations maintained at <1 ppm. Four electrodes were measured in order to have a sufficient interaction volume with the x-ray beam. Stacked electrodes were placed in the sample chamber that was filled with He gas, transported to the beamline under inert atmosphere. A Silicon (311) monochromator was used to scan the incident energy while analyzers near the backscatter (555) diffraction condition were used to resolve the scattered x-rays.[31] A series of scans at the elastic energy of 9890.4 eV were performed in order to optimize the signal attained at each detector prior to scanning the C K-edge with a step size of 2 eV in the pre-edge region, 0.1 eV close to the edge, and 3 eV in the fine structure region. A q range of 0.6-8 $Å^{-1}$ was measured, and the resulting spectra were averaged across the different detectors. Five scans were measured for each sample, calibrated to the energy loss scale, and averaged. Data were processed by fitting the edges with an arctangent function and Gaussian function, optimized using a least squares regression algorithm. Background was subtracted by removing the resulting Gaussian function.

COMPUTATIONAL METHODS

The electronic structure of intercalated graphite was modeled using density functional theory (DFT) with WIEN2k (version 17.1), an all-electron, full-potential commercially available software package, which uses linearized plane waves with local orbitals in a Kohn-Sham scheme.[32] The calculations were performed using the Perdew, Burke and Ernzerhof generalized gradient approximation (PBE-GGA) exchange-correlation functional.[33] An $R_{MT} K_{MAX}$= 8.0 was used in all calculations, and the k-mesh was selected so that the total energy per unit cell was stable to within 10^{-5} Ry. For graphite, this corresponds to a 25x25x7 k-mesh. For supercells correspondingly smaller k-meshes were used.

Graphite, with and without intercalants, was modeled using DFT and three models were considered. First, pure graphite with its preferred AB stacking was considered. This was compared to a second model, an identical structure but with PF_6 added between every two layers of graphite (henceforth referred to as stage 2 intercalated graphite. The graphite interlayer separation was taken from literature values,[1] and the PF_6 gallery height of 4.47 Å was taken from previously reported values in the literature,[15] which were confirmed by XRD here (Figure S1). The PF_6 molecule was oriented so that three fluorine atoms are centered in the carbon rings below the P atom, and three above the P atom. To model this, a 4x2x1 supercell of AB graphite was used, and the c-axis of the crystal was extended to accommodate the PF_6 molecules. A packing of 1 PF_6 molecule per 32 atoms was considered, close to the experimental value of 0.23 PF_6^- ions per C_6 unit observed from coulometry after galvanostatic charging of the graphite cathode to 5.2 V vs. Li^+/Li^0 (Figure S2). After allowing the structure to relax, a final crystal structure was obtained. Finally, to distinguish changes to the electronic properties of the system due structural changes induced by the intercalant from additional changes due to interaction between the graphite host lattice and the intercalant, a third system was considered in which PF_6 molecules were removed from the intercalated lattice, but the interlayer spacing of the charged state was preserved.

The DFT calculations were used to calculate both the density of states as well as the predicted C K XANES and XES spectra, allowing for a direct, detailed comparison with experiment. The spectra were calculated by multiplying the partial density of states by a dipole transition matrix and a radial transition probability.[34] The calculated spectra were broadened using a combination of Lorentzian and Gaussian lineshapes reflecting lifetime and instrumentation-related broadening, respectively. The XANES and XES spectra depend on the final state of the system for that measurement. In XANES, it corresponds to a crystal perturbed by the presence of a core hole,[35,36] which tends to shift spectral weight to lower energies. To account for this perturbation, a XANES spectrum was calculated for each unique carbon atom by adding half a core hole to that site. For the case of graphite a 4x2x1 supercell was used so that adjacent fractional core holes are separated by at least 4.9 Å.

RESULTS AND DISCUSSION

The representative electrochemical response of graphite when used as a cathode for PF_6 intercalation (Figure S2), and the corresponding changes in XRD (Figure S1), were consistent with the literature, indicating that the desired compositions were achieved. The different plateaus that form during cycling of these compounds have been attributed to the formation of different stages of graphite as higher concentrations of intercalant are introduced. Further details on the structural transformations involved in these steps, the reader is referred to existing studies the literature.[15,16] There was no significant difference between HOPG and MCMB electrodes. To explore the effect of intercalation of PF_6^- in the bulk of graphite without interference from surface species, C K-edge XRS spectra were collected of pristine HOPG and HOPG after charging to 5.2 V vs. Li^+/Li shown in Figure 1, panels (a) and (c). In these spectra, four features have been labeled 1-4, as shown. The pristine HOPG showed two principal features, the π^* (at 285.4 eV) and σ^* peaks (at 292.0 eV), labeled as 2 and 4, respectively. Their position and relative intensity were consistent with literature reports.[37] Upon anion intercalation, two significant changes were observed. First, a pre-π^* feature emerged, labeled as 1. Second, the π^* feature shifted to a higher energy by 0.2 eV, labeled as feature 3. The σ^* peak remained largely unchanged. MCMB powders are more relevant to the ultimate application in a battery, as HOPG is not suitable for processing following industry standards. However, MCMB electrodes could not be measured by XRS because optimal XRS signal is attained when the sample thickness is greater than the penetration length of the incident x-rays. For carbon at 10 keV, this length is approximately 2 mm, 25 times thicker than an MCMB electrode, rendering the measurement unfeasible. Instead, the C K-edge XANES of pristine and charged HOPG were compared to MCMB electrodes in the right panel of Figure 2. These spectra were collected using a TEY detector, which probes ~10 nm into the surface of the material,[38] and, therefore, requires small amounts of sample, but also leads to convolution of

species resulting from interfacial interactions with the environment inside the battery. Comparing the XANES data in the right panel of Figure 2 to the XRS data in Figure 1, the same principal features and changes were observed.

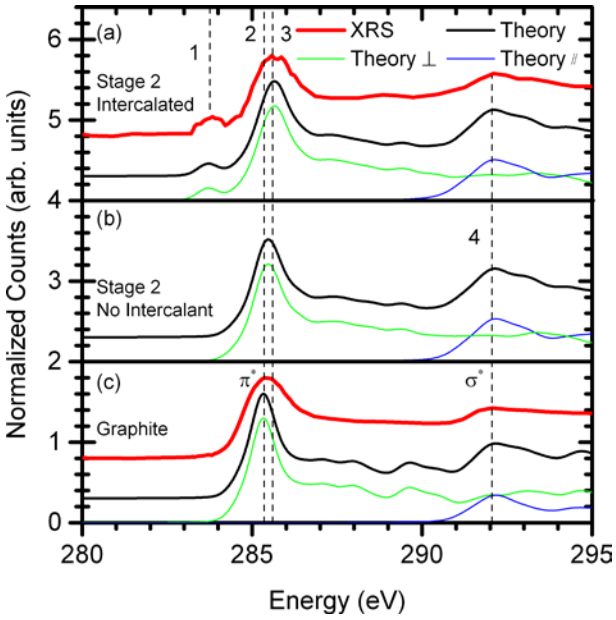

Figure 1. XRS and calculated XRS spectra for (a) stage 2 PF_6 intercalated graphite, (b) stage 2 intercalated graphite without intercalant, and (c) AB-stacked graphite. For (a) and (c) the XRS spectra are shown in a thick red line. For each case the overall calculated spectrum is shown, as well as the out-of-plane (⊥) and in-plane (∥) contributions, are shown using narrow lines as indicated in the legend. Spectra are vertically offset for visual clarity.

Electrochemical charging resulted in the growth of feature 1, a pre-π* feature, a shift of the π* feature to a higher energy, and a relatively unchanged σ* peak. Therefore, it is key to note that the redistribution of spectral weight reflects a characteristic change of the electronic properties throughout this system induced by anion intercalation, irrespective of crystal morphology or size. Furthermore, the fact that similar spectral weight redistribution is present in both HOPG and MCMB suggests that this change is insensitive to changes in graphite disorder, the principal difference between these materials. The subtle differences in relative intensities of these peaks measured in XANES and XRS spectra do not necessarily reflect intrinsic changes in the material, but rather the different sensitivity of the XANES and XRS spectra in this work to in-plane and out-of-plane C 2*p* states due to subtle differences in sample-beam geometry in the measurement combined with the dichroism of graphite. Here we used an experimental geometry of incident radiation 35° from the surface for XANES in order to get a strong contribution from both π* and σ* peaks, but similar control over XRS geometry is more difficult to attain. In XRS, the incident radiation comes at a low angle (approximately 10° from the surface) and the energy loss spectra are collected from all 19 detectors located at different angles and averaged. A subtle difference between the XANES and XRS occurs with the σ* splitting at 292.7 eV. This splitting, which is characteristic of graphite in TEY XANES spectra, is not reproduced in the XRS measurements. Other

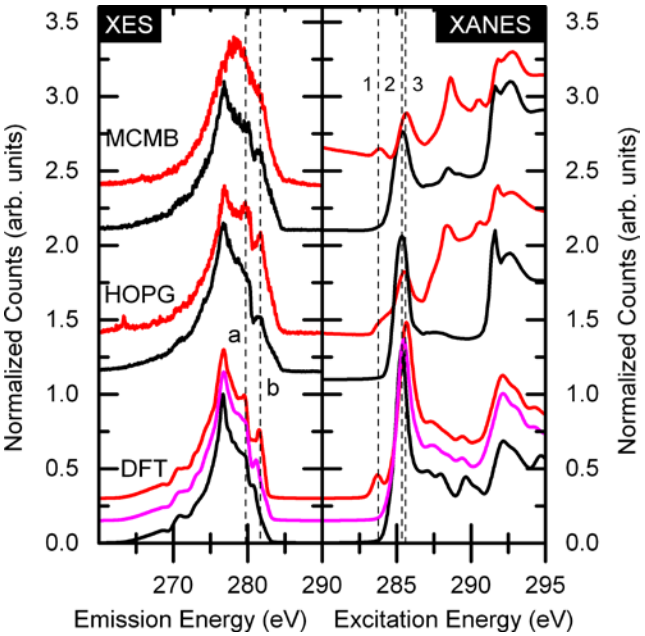

Figure 2. C K x-ray emission and TEY absorption spectra are shown in the left and right panels, respectively. Measured spectra are shown for HOPG and MCMB, as indicated, together with DFT calculated spectra. For each type of graphite, pristine and maximally intercalated spectra are shown in black and red, respectively. For the calculated spectra, black, magenta and red lines correspond to pristine, stage 2 no intercalant and stage 2 intercalated graphite, respectively.

studies suggest that the absence of these features is characteristic of this technique.[39,40] The DFT calculations reproduce well the XRS spectra, but the prominence of the splitting in the XANES spectra is not reproduced. The agreement of the DFT with the XRS spectra and disagreement of the DFT with the XANES spectra suggests that the prominence of this feature is exaggerated in the XANES spectra. Examining the calculated in-plane and out-of-plane contributions to the overall spectral shape suggests that sample orientation effects cannot explain this discrepancy. Lastly, the only meaningful difference between XANES and XRS lied in the region between π* and σ* peaks, in which charging induced a growth of a new peak at 288 eV, accompanied by a smaller feature at 290 eV. Peaks at this energy have been associated with carbon species with oxygen functional groups (e.g., -COO^-) at electrode surfaces, which can form due to side-reactions with the electrolyte at high redox potentials.[15] This notion is supported by the presence of these peaks in TEY and not XRS, given their very different probing depths, and further supported by the fact that DFT does not predict such substantial peak intensity between the π* and σ* regions (see below).

To interpret the x-ray spectra, this system was modeled using DFT, shown in Figure 1. The theoretical XANES/XRS spectra of pristine graphite was compared with an artificial graphite state with an interlayer distance corresponding to stage II, but no intercalant, as well as AB-stacked graphite forming stage II as a result of the presence of PF_6^-. In the latter case, a composition $(PF_6)_{0.1875}C_6$ (or $[PF_6]C_{32}$) was chosen based on the capacity measured from the electrochemical cell after charging

of the graphite cathode to 5.2 V vs. Li^+/Li^0, equivalent to 0.18-0.2 mol PF_6 per C_6 unit (Figure S2). A stage II structure was chosen following analysis of this and similar anion GICs in the literature,[15,41] which assumes that only the anion, without solvent molecules, is present in the interlayer spacing. The ratio of the out-of-plane and in-plane spectral weight was weighted to reflect the experimental conditions. These spectra reflect a system perturbed by a core-hole, as discussed in the modeling section. Considering the pristine HOPG spectrum, it is clear that the π^* and σ^* features are due to core transitions with out-of-plane and in-plane C p states, respectively. The presence of a core hole has the effect of redistributing spectral weight to lower energies (shown in Figure S3), resulting in a sharpening of the π^* feature, but not the emergence of any pre-π^* features.

The important observation is that when comparing the calculated system with PF_6^- intercalant and the corresponding XRS spectrum, the same two principal changes seen in experiment are reproduced: a new pre-π^* feature emerges and the π^* feature shifts upward by 0.2 eV, with all major features appearing at the correct position and with the correct intensity. After decomposing the in-plane and out-of-plane contributions to the calculated spectrum (see blue versus green lines in Figure 1), it is clear that the pre-π^* feature is due to out-of-plane C 2*p* states. This finding is supported by the momentum transfer dependence of the XRS spectra (Figure 1), where this feature had a similar momentum transfer sensitivity as the π^* feature. Considering a system with the same carbon structural arrangement and spacing as stage 2, but without intercalant molecules (Figure 1(b)), there are two points of note. First, the distortion of the graphite lattice is insufficient to introduce a pre-π^* feature, which requires the electronic effects introduced by the presence of the negatively charged intercalant. This observation suggests that the co-intercalation of neutral molecules, such as from the solvent,[42] would not have a strong effect on these electronic signatures because they would only affect interlayer spacing. Second, the position of the π^* feature is between the same features in the computed spectra of pristine and intercalated graphite.

To evaluate the changes of the occupied density of states as a function of anion intercalation, the XES spectra were collected, shown in the left panel of Figure 2 In the spectra of HOPG increasing spectral weight is seen at the highest energy features at 279.6 eV and 281.7 eV, labeled as a and b, respectively upon charging. Similar changes are seen in intercalated MCMB, although upon intercalation this sample appears to become more atomically disordered because the signals (and associated electronic states) became more washed out than in HOPG.

To better understand the origin of the pre-π^* feature, as well as the changes in the XES spectral weight, we consider the DFT calculation in more detail. As described in the calculation details section, to model stage 2 intercalated graphite, PF_6 molecules were introduced between graphite layers with a spacing corresponding to known experimental values.[15,16]

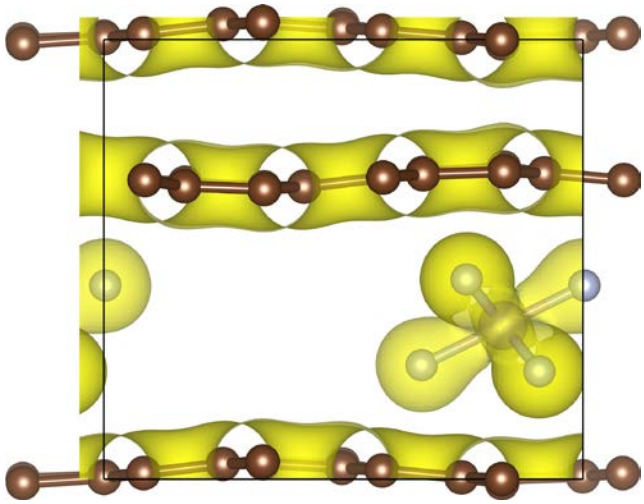

Figure 3. A diagram showing the relaxed structure of stage 2, PF_6-intercalated AB-graphite, with carbon, fluorine and phosphorous atoms shown as brown, grey and pink spheres, respectively. A surface of constant charge density of the valence band in this material is shown in yellow.

After an initial structural input, the system was allowed to relax, resulting in the structure shown in Figure 3. Owing to the relatively low gallery height of PF_6, the spacing between carbon layers near the PF_6 molecule diminishes, resulting in a stretching of the C-C nearest neighbor distances, and a less ordered graphite layer. This effect reduces crystallographic order, especially on the *ab* crystallographic plane, thus being consistent with the loss of intensity in the XRD patterns upon anion intercalation during charging, as can be seen in Figure S1.

The electronic band structure diagram for AB graphite, expanded (stage 2-like) graphite without intercalant, and stage 2 graphite with PF_6 anions can be seen in Figure 4. The agreement between computed and experimental spectra support the changes in the diagram observed upon intercalation. Comparing the AB graphite and its expanded counterpart without intercalant, despite the general similarity, a slight redistribution of states was observed in the latter crystal, reflecting perturbations to the lattice (An example of these changes can be seen by considering states near the Gamma point in the vicinity of -8 eV). Introducing the intercalant results in two notable additional changes. First, compared to AB graphite, the Fermi energy level is lowered by 0.60 eV, as can be seen by considering the band crossing at the K-point at the Fermi level in the case of AB graphite. Qualitatively, this lowering of the Fermi level suggests that charge is removed from the carbon host lattice upon intercalation, resulting in oxidized carbon layers. Quantitatively, a Bader analysis of charge in this system shows that on average each carbon atom has a net charge of $0.030|e|$, an average fluorine atom has a net charge of $-0.811|e|$, and a phosphorous atom has a net charge of $3.933|e|$. Taken together, the calculations produce an overall net charge for each PF_6 molecule of $-0.932|e|$, close to the formal chemical charge state of $-1|e|$, and reflect the expected covalence in the P-F bond. The fact that the formal charge of PF_6^- is preserved after intercalation is consistent with the similarity between P K- and F K-edge XANES collected from the charged electrode and a standard of $LiPF_6$, which has a strong ionic character (Figure S4, S5). Further, the net charge in each carbon atom matches well with the expected charge distribution in $(PF_6^-)_{0.2}(C_6)^{0.2+}$, the final state after cathode charging, according to coulometry (Figure S2). Putting this

together, the origin of the pre-π^* feature in the XRS and XANES spectra upon anion intercalation is due to the removal of electronic charge from the graphite host to compensate the intercalation of an anion. The result is an effective lowering of the Fermi energy level or, put differently, an emptying of previously occupied states. These newly empty states, being unoccupied, can therefore be detected using XRS and XANES, leading to the pre-π^* feature. Although these calculations were on PF_6^-intercalated graphite, this effective lowering of the Fermi energy level is a general result which is expected to occur for other anions intercalated into graphite, provided that the host lattice remains graphitic. Since the XRS and XANES measurements are sensitive to changes in the Fermi energy level, which depend on the degree of transfer of electronic charge from the host lattice, this result is expected to be independent of the formal stage index. This effective lowering of the Fermi energy level has been observed in our calculations involving other anions (BF_4^- and ClO_4^-, not shown). The shift of the π^* feature by 0.2 eV upon intercalation can be understood qualitatively from a simple effective nuclear charge electrostatic model. Since the carbon atoms are oxidized upon intercalation, the effective nuclear charge increases, increasing the energy required to excite a core electron to the π^* energy level.

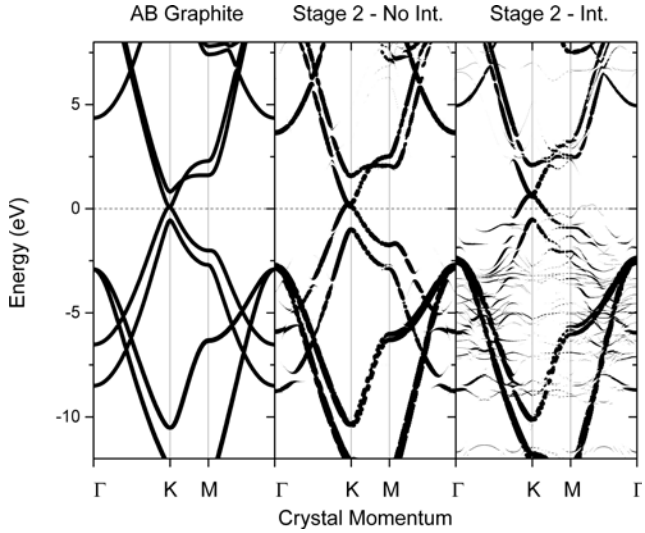

Figure 4. (left) An electronic band structure diagram of AB-graphite of a path through the Brillouin zone. (middle, right) An energy-crystal momentum diagram of the Bloch spectral weight of the stage 2 intercalated without intercalant and stage 2 intercalated models, respectively for a path which matches the one shown in the left panel. The point size corresponds to the Bloch weight.

The relative sharpness of the pre-π^* feature, distinct from the rest of the conduction band, in the XANES and XRS spectra, can also be understood from the band structure diagram of the intercalated system. For a two-dimensional system with a linear band dispersion and Fermi energy crossing at a high symmetry point in the Brillouin zone, such as graphene, the density of states has a linear dependence on energy, with zero states at the Fermi energy level. For the intercalated graphite case, we see that in the vicinity of the band crossing at the *K* point at 0.60 eV, the band dispersion is approximately linear. This results in a minimum in the density of states at this crossing point, and a related reduction in XANES/XRS spectral weight. Although the XANES and XRS spectra are perturbed by the presence of a core hole, the pre-π^* feature remains clearly distinguishable. A comparison of XANES/XRS spectra with and without a core hole is shown in Figure S3. The minimum in density of states of the intercalated system is now well above the Fermi energy level, resulting in a density of occupied states near the Fermi level which is greater than in AB graphite. This leads to an increase in spectral weight at the high energy region of the XES spectra for the intercalated in this region.

The second change in the electronic band structure of graphite upon intercalation of PF_6^- is the appearance of many additional dispersive bands. Their dispersive nature suggests that these states are relatively localized, consistent with their molecular origin. An isocontour of the valence band charge is shown in Figure 3, which shows that although the graphite charge density of the carbon atoms all overlap, the PF_6 charge density is localized around the molecule. Finally, since the Fermi energy level occurs at an energy with continuous bands, the intercalated graphite remains metallic, a favorable physical property in view of its used as an electrode, where electrons must flow within the bulk of the active material.

The emergence of pre-π^* XANES spectral weight in graphite has been previously observed in $FeCl_3$ intercalated graphite[27] and substitutional boron doped graphite.[4] What these cases have in common is that the intercalant or dopant acts as an electron acceptor, which results in an effective lowering of the Fermi energy level since electrons are removed from the host lattice. The same phenomenon has been observed in intercalated nanotubes.[28] In these prior works, the pre-π^* feature was interpreted as a lowering of the Fermi energy level, and this phenomenon has been previously predicted in DFT studies,[43] but this work unambiguously demonstrates this phenomenon. When graphite is intercalated with an electron donor, such as Li, a reduction in spectral weight at the onset of the π^* feature is observed.[39]

CONCLUSIONS

The changes in electronic structure of graphite upon electrochemical intercalation of PF_6^- in a battery have been studied using techniques sensitive to the occupied and unoccupied partial density of states, together with complementary DFT calculations. This work reveals the emergence of a pre-π^* feature, experimentally observed by XRS/XANES, due to the generation of new unoccupied states upon oxidation of the carbon lattice, resulting in a lowering of the Fermi energy level of 0.60 eV. A similar lowering of the Fermi energy has been calculated for other intercalant anions (BF_4^- and ClO_4^-). The match between experimental and computational observations reveals important aspects of bonding and electron distribution after intercalation. The analysis reveals an ionic interaction between the graphite structure and interlayer PF_6^- ions, with the charge compensation in the electrode reaction occurring primarily at C atoms. However, the band structure of the graphite intercalation compound remains free of a band gap, indicating that it remains metallic. These observations indicate that the flow of electrons should remain facile along the stacked graphene sheets. The ionic interaction occurs and a large negative charge (PF_6^-) and a highly delocalized positive charge are formed in the carbon network, which could lead to weak electrostatic interactions that favor the mobility of the anion to move within the lattice at room temperature, consistent with recent measurements of elec-

trochemical reaction kinetics. These aspects have important implications for the functionality of this reaction as the storage mechanism in the cathode of a dual carbon battery and it is likely to translate to other anions of interest in multivalent electrochemical devices, such as BF_4^- and ClO_4^-. They broadly increase our understanding of how the physics of carbonaceous materials can be manipulated by intercalation.

ASSOCIATED CONTENT

Supporting Information

The Supporting Information is available free of charge on the ACS Publications website.

Powder x-ray diffraction data; electrochemical response of graphite electrodes; calculated XANES spectra; P K-edge and F K-edge XANES data (PDF)

AUTHOR INFORMATION

Corresponding Author

* tristan.deboer@usask.ca
* jcabana@uic.edu

Author Contributions

The manuscript was written through contributions of all authors. All authors have given approval to the final version of the manuscript.

ACKNOWLEDGMENT

We acknowledge support from NSERC and the Canada Research Chair program. This research used resources of the Advanced Photon Source, a U.S. Department of Energy (DOE) Office of Science User Facility operated for the DOE Office of Science by Argonne National Laboratory under Contract No. DE-AC02-06CH11357. This research used resources of the Advanced Light Source, which is a DOE Office of Science User Facility under contract no. DE-AC02-05CH11231. The computational component of this work was enabled by resources provided by Compute Canada Calcul Canada (www.computecanada.ca) and the Plato computing cluster at the University of Saskatchewan.

REFERENCES

(1) Chung, D. D. L. Review Graphite. *J. Mater. Sci.* **2002**, 37, 1475-1489.

(2) Hunt, A.; Kurmaev, E. Z.; Moewes, A. A Re-evaluation of How Functional Groups Modify the Electronic Structure of Graphene Oxide. *Adv. Mater. (Weinheim, Ger.)* ***2014***, 26, 4870–4874.

(3) Ketabi, N.; de Boer, T.; Karakaya, M.; Zhu, J.; Podila, R.; Rao, A. M.; Kurmaev, E. Z.; Moewes, A. Tuning the electronic structure of graphene through nitrogen doping: experiment and theory. *RSC Adv.* **2016**, 6, 56721-56727.

(4) Hanafusa, A; Muramatsu, Y.; Kaburagi, Y.; Yoshida, A.; Hishiyama, Y.; Yang, W.; Denlinger, J. D.; Gullikson, E. M. Local structure analysis of boron-doped graphite by soft x-ray emission and absorption spectroscopy using synchrotron radiation. *J. Appl. Phys. (Melville, NY, U. S.)* **2011**,110. 53504.

(5) Dresselhaus, M. S.; Dresselhaus, G. Intercalation compounds of graphite.*Adv. Phys.* **2002**, 51, 1–186, Jan. 2002.

(6) Xu, J.; Dou, Y.; Wei, Z.; Ma, J.; Deng, Y.; Li, Y.; Liu, H.; Dou, S. Recent Progress in Graphite Intercalation Compounds for Rechargeable Metal (Li, Na, K, Al)-Ion Batteries. *Adv. Sci. (Weinheim, Ger.)* **2017**, 4, 1700146.

(7) Entani, S.; Ikeda, S.; Kiguchi, M.; Saiki, K.; Yoshikawa, G.; Nakai, I.; Kondoh, H.; Ohta, T. Growth of nanographite on Pt(111) and its edge state. *Appl. Phys. Lett.* **2006**, 88, 153126.

(8) Etacheri, V.; Marom, R.; Elazari, R.; Salitra, G.; Aurbach, D. Challenges in the Development of Advanced Li-ion Batteries: a Review. *Energy Environ. Sci.* **2011**, 4, 3243-3262.

(9) Read, J. A.; Cresce, A. V.; Ervin, M. H.; Xu, K. Dual-Graphite Chemistry Enabled by a High Voltage Electrolyte. *Energy Environ. Sci.* **2014**, 7, 617–620.

(10) Ishihara, T.; Koga, M.; Matsumoto, H.; Yoshio, M. Electrochemical Intercalation of Hexafluorophosphate Anion into Various Carbons for Cathode of Dual-Carbon Rechargeable Battery. *Electrochem. Solid-State Lett.* **2007**, 10, A74-A76.

(11) Rodríguez-Pérez, I. A.; Ji, X. Anion Hosting Cathodes in Dual-Ion Batteries. *ACS Energy Lett.* **2017**, 2, 1762–1770.

(12) Rothermel, S.; Meister, P.; Schmuelling, G.; Fromm, O.; Meyer, H.-W.; Nowak, S.; Winter, M.; Placke, T. Dual-Graphite Cells based on the Reversible Intercalation of Bis(Trifluoromethanesulfonyl)imide Anions from an Ionic Liquid Electrolyte. *Energy Environ. Sci.* **2014**, 7, 3412–3423.

(13) Lin, M. C.; Gong, M.; Lu, B.; Wu, Y.; Wang, D. Y.; Guan, M.; Angell, M.; Chen, C.; Yang, J.; Hwang, B. J.; Dai, H. An Ultrafast Rechargeable Aluminium-Ion Battery. *Nature (London, U. K.)* **2015**, 520, 325–328.

(14) Li, Q.; Bjerrum, N. J. Aluminum as anode for energy storage and conversion: a review. *J. Power Sources* **2002**, 110, 1–10.

(15) Seel, J. A.; Dahn, J. R. Electrochemical Intercalation of PF6 into Graphite. *J. Electrochem. Soc.* **2000**, 147, p. 892-898.

(16) Read, J. A. In-Situ Studies on the Electrochemical Intercalation of Hexafluorophosphate Anion in Graphite with Selective Cointercalation of Solvent. *J. Phys. Chem. C* **2015**, 119, 8438–8446.

(17) Miyoshi, S.; Akbay, T.; Kurihara, T.; Fukuda, T.; Staykov, A. T.; Ida, S.; Ishihara, T. Fast Diffusivity of PF_6 – Anions in Graphitic Carbon for a Dual-Carbon Rechargeable Battery with Superior Rate Property. *J. Phys. Chem. C* **2016**, 120, 22887–22894.

(18) Tasaki, K. Density Functional Theory Study on Structural and Energetic Characteristics of Graphite Intercalation Compounds. *J. Phys. Chem. C* **2014**, 118, 1443–1450.

(19) Zhang, Z. Electrochemical Oxidation of Graphite in Organic Electrolytes Containing PF_6^- or ClO_4^-. *J. Electrochem. Soc.* **1993**, 140, 742-746.

(20) Billaud, D. Electrochemical Intercalation of Fluorides into Pyrographite. *J. Power Sources* **1984**, 13, 1–7.

(21) Billaud, D.; Pron, A.; Lincoln Vogel, F.; Hérold, A. Intercalation of Pyrographite by NO_2^+ and NO^+ Salts. *Mater. Res. Bull.* **1980**, 15, 1627–1634.

(22) Fan, H.; Qi, L.; Yoshio, M.; Wang, H. Hexafluorophosphate Intercalation into Graphite Electrode from Ethylene Carbonate/Ethylmethyl Carbonate. *Solid State Ionics* **2017**, 304, 107–112.

(23) Fan, H.; Qi, L.; Wang, H. Hexafluorophosphate Anion Intercalation into Graphite Electrode from Methyl Propionate *Solid State Ionics* **2017**, 300, 169–174.

(24) Gao, J.; Tian, S.; Qi, L.; Yoshio, M.; Wang, H. Hexafluorophosphate Intercalation into Graphite Electrode from Gamma-Butyrolactone Solutions in Activated Carbon/Graphite Capacitors *J. Power Sources* **2015**, 297, 121–126.

(25) de Groot, F.; Kotani, A. *Core Level Spectroscopy of Solids*. CRC Press, Boca Raton, FL, USA **2008**.

(26) Zhou, S. Y.; Girit, Ç. Ö.; Scholl, A.; Jozwiak, C. J.; Siegel, D. A.; Yu, P.; Robinson, J. T.; Wang, F.; Zettl, A.; Lanzara, A. Instability of Two-Dimensional Graphene: Breaking sp^2 Bonds with Soft X-rays. *Phys. Rev. B* **2009**, 80, 121409(R)(1-8).

(27) Mele, E. J.; Ritsko, J. J. Fermi-Level Lowering and the Core Exciton Spectrum of Intercalated Graphite. *Phys. Rev. Lett.* **1979**, 43, 68–71.

(28) Liu, X.; Pichler, T.; Knupfer, M.; Fink, J.; Kataura, H. Electronic Properties of $FeCl_3$-Intercalated Single-Wall Carbon Nanotubes *Phys. Rev. B* **2004**, 70, 205405(1-5).

(29) Toby, B. H.; Von Dreele, R. B. GSAS-II: The Genesis of a Modern Open-Source All Purpose Crystallography Software Package *J. Appl. Crystallogr.* **2013**, 46, 544–549.

(30) Pawley, G. S. Unit-Cell Refinement from Powder Diffraction Scans. *J. Appl. Crystallogr.* **1981**, 14, 357–361.

(31) Fister, T. T.; Seidler, G. T.; Wharton, L.; Battle, A. R.; Ellis, T. B.; Cross, J. O.; Macrander, A. T.; Elam, W. T.; Tyson, T. A.; Qian, Q. Multielement spectrometer for efficient measurement of the momentum transfer dependence of inelastic x-ray scattering. *Rev. Sci. Instrum.* **2006**, 77, 63901(1-7).

(32) Blaha, P.; Schwarz, K.; Madsen, G. K. H.; Kvasnicka, D.; Luitz, J.; Laskowski, R.; Tran, F.; Marks, L. D. *WIEN2k, An Augmented Plane Wave + Local Orbitals Program for Calculating Crystal Properties*. Techn. Universität Wien, Wien, Austria **2018.**

(33) Perdew, J.; Burke, K.; Wang, Y. Generalized Gradient Approximation for the Exchange-Correlation Hole of a Many-Electron System. *Phys. Rev. B* **1996**, 54, 16533–16539.

(34) Schwarz, K.; Neckel, A.; Nordgren, J. On the X-ray Emission Spectra from FeAl. *J. Phys. F: Met. Phys.* **1979**, 9, 2509-2521.

(35) Mahan, G. Final-State Potential in X-ray Spectra. *Phys. Rev. B* **1980**, 21, 1421-1431.

(36) Von Barth, U.; Grossmann, G. Dynamical Effects in X-Ray Spectra and the Final-State Rule. *Phys. Rev. B* **1982**, 25, 5150-5179.

(37) Denley, D.; Perfetti, P.; Williams, R. S.; Shirley, D. A.; Stöhr, J. Carbon K-edge Fine Structure in Graphite Foils and in Thin-Film Contaminants on Metal Surfaces. *Phys. Rev. B* **1980**, 21, 2267-2273.

(38) Abbate, M.; Goedkoop, J. B.; de Groot, F. M. F.; Grioni, M.; Fuggle, J. C.; Hofmann, S.; Petersen, H.; Sacchi, M. Probing Depth of Soft X-ray Absorption Spectroscopy Measured in Total-electron-yield mode. Surf. Interface Anal. **1992**, 18, 65-69.

(39) Boesenberg, U.; Sokaras, D.; Nordlund, D.; Weng, T. C.; Gorelov, E.; Richardson, T. J.; Kostecki, R.; Cabana, J. Electronic Structure Changes upon Lithium Intercalation into Graphite – Insights from *Ex Situ* and *Operando* X-ray Raman Spectroscopy. *Carbon* **2019**, 143, 371–377.

(40) Cavallari, C.; Brunelli, M.; Radescu, S.; Dubois, M.; Batisse, N.; Vaughan, G. B. M.; Fischer, H. E.; Pischedda, V. Structural and Electronic Changes in Graphite Fluorides as a Function of Fluorination Rate: An XRS, PDF and DFT Study. *Carbon N. Y.* **2019**, *147*, 1–8.

(41) Jobert, A.; Touzain, P.; Bonnetain, L. Insertion des Ions PF_6^-, AsF_6^- et SbF_6^- dans le Graphite par Methode Electrochimique. Caracterisation des Produits Obtenus. *Carbon* **1981**, 19, 193–198.

(42) Li, Y.; Lu, Y.; Adelhelm, P.; Titirici, M.-M.; Hu, Y.-S. Intercalation Chemistry of Graphite: Alkali Metal Ions and Beyond. *Chem. Soc. Rev.* **2019**, 48, 4655-4687.

(43) Kim, N.; Kim, K. S.; Jung, N.; Brus, L.; Kim, P. Synthesis and Electrical Characterization of Magnetic Bilayer Graphene Intercalate. *Nano Lett.* **2011**, 11, 860–865.

Table of Contents Graphic